



# Simultaneous capturing of mixed contaminants from wastewater using novel one-pot chitosan functionalized with EDTA and graphene oxide adsorbent<sup>☆</sup>

Monu Verma<sup>a</sup>, Ashwani Kumar<sup>b</sup>, Ingyu Lee<sup>a</sup>, Vinod Kumar<sup>c,d</sup>, Ju-Hyun Park<sup>e</sup>, Hyunook Kim<sup>a,\*</sup>

<sup>a</sup> Water-Energy Nexus Laboratory, Department of Environmental Engineering, University of Seoul, Seoul, 02504, Republic of Korea

<sup>b</sup> Institute Instrumentation Centre (IIC), Indian Institute of Technology Roorkee, Roorkee, 247667, India

<sup>c</sup> Peoples' Friendship University of Russia (RUDN University), Moscow, 117198, Russian Federation

<sup>d</sup> Department of Life Sciences, Graphic Era (Deemed to Be University), Dehradun, Uttarakhand, 248002, India

<sup>e</sup> National Institute of Environmental Research, Ministry of Environment, 42 Hwangyeong-ro, Seo-gu, Incheon, 22689, South Korea

## ARTICLE INFO

### Keywords:

Ciprofloxacin  
Heavy metal ions  
Mixed contaminants  
Multifunctional chitosan  
Recyclability  
Wastewater treatment

## ABSTRACT

The emergence of inorganic and organic contaminants has raised great concerns owing to their adverse impact on human health and ecological security. Herein, first time one-pot process was applied for chitosan (CS) functionalization using graphene oxide (GO) and ethylenediaminetetraacetic acid (EDTA) for simultaneous capturing of toxic inorganic (lead (Pb<sup>2+</sup>) and cadmium (Cd<sup>2+</sup>)) and organic (ciprofloxacin (CIP) and sildenafil (SDF)) contaminants from wastewater. In this approach, we believe that CS would work as a backbone, GO would capture both inorganic and organic contaminants via electrostatic interactions, while EDTA would make complexation with heavy metals. Various parameters including pH, reaction time, concentration, reusability etc. were evaluated to achieve the best experimental result in monocomponent system. The prepared adsorbent displayed an excellent monolayer adsorption capacity of 351.20 and 264.10 mg g<sup>-1</sup> for Pb<sup>2+</sup> and Cd<sup>2+</sup>, respectively, while a heterogeneous sorption capacity of 75.40 and 40.90 mg g<sup>-1</sup> for CIP and SDF, respectively. The kinetics data fitted well to Pseudo-second order (PSO) kinetics model for both types of contaminants and gave faster interaction towards metal ions (higher k<sub>2</sub>) than organic contaminants. Experimental results showed excellent adsorption efficiencies at environmental levels in the capturing of both inorganic and organic contaminants at the same time from polluted water. The capturing mechanism of both types of contaminants was explained by elemental mapping, EDS, and FT-IR spectra. Overall, easy synthesis, excellent capturing capacity, and reusability imply that the prepared adsorbent has a sufficient potential for the treatment of co-existing toxic contaminants in water.

## 1. Introduction

Recently, rapid development of human society and industries throughout the world, different types of environmental problems such as inorganic and organic contaminants in water body create a threat to the human health and aquatic ecosystems. These contaminants discharged from a wide range of sources such as households, agriculture, traffic networks or different industries and enter in the water bodies through diverse entry paths (Li et al., 2022; Verma et al., 2021b; Wen et al., 2017). Among them, heavy metals and pharmaceutical drugs are the most emerging contaminants which potentially have a serious threatening effect

to human and animal health and to the surface water environment as well as groundwater (Chen et al., 2019a). Therefore, effective treatment of contaminated water before releasing into the environment is necessary. Among the different traditional treatment methods, adsorption is regarded as one of the most cost-effective method to remove the contaminants from wastewater due to its simple function, low cost and wide applicability for different contaminants (Hu et al., 2020; Verma et al., 2021c). Till now, different types of adsorbents such as activated carbon, clay based materials, polymeric adsorbents (Ajiboye et al., 2021), modified chitosan (CS) (Guo et al., 2018), magnetic sewage sludge biochar (MSSBC) (Ifthikar et al., 2017), calixarene-based porous organic

<sup>☆</sup> This paper has been recommended for acceptance by Jörg Rinklebe

\* Corresponding author.

E-mail address: [h\\_kim@uos.ac.kr](mailto:h_kim@uos.ac.kr) (H. Kim).

polymers (POPs), DMPillar[5]arene-based porous organic polymer (DMPBP[5]) (Yang et al., 2021a) etc. have been used to capture metallic ions and organic dyes from wastewater. Nonetheless, these adsorbents have shown a good adsorption capacity for individual inorganic or organic contaminants only. Therefore, it is urgently needed to synthesize new adsorbing material to capture both heavy metals as well as organic contaminants from wastewater.

Chitosan, a well-known polysaccharide biopolymer derived from the alkaline deacetylation of chitin in nature, is widely used as an adsorbent for capturing inorganic (e.g., metal ions) and organic contaminants from wastewater (Cho et al., 2021; Yang et al., 2021b). It has merits of non-toxicity, low cost, biocompatibility, and biodegradability, so it has been chosen in a variety of applications. CS has a huge number of  $-NH_2$ / $=NH$  and  $-OH$  groups on its molecular chains which makes it highly selective material for the capturing of metal ions and pharmaceutical drugs through hydrogen bonding and chelation (Usman et al., 2021; Vakili et al., 2019). However, solubility in acid solution, poor chemical resistance, swelling in aqueous solution, and difficulty in separation by common methods are the issues with CS in capturing of contaminants from wastewater. Many significant efforts were applied to overcome these drawbacks in the synthesis of CS-based hybrid adsorbents; a common approach is using glutaraldehyde (GA), ethylene-bis (oxyethylenetriamino)tetraacetic acid, ethylenediaminetetraacetic acid (EDTA) or epichlorohydrin (EPI) as a crosslinking agent for the capturing of inorganic and organic contaminants with higher adsorption capacities (Marrakchi et al., 2020; Wang et al., 2017; Zhao et al., 2013). However, GA and EPI are highly toxic and possess immunogenicity or carcinogenicity nature towards human beings and animals (Reddy and Lee, 2013). Apart from them, many composites of CS and others, such as thiol cross-linked composite with sludge biochar (CSC@SDBC), core-shell SBA-dithiocarbamate CS composite (CS<sub>2</sub>C@SBA-3), sewage sludge derived carbon-supported Mg(II) composite (SDBC-Mg(II)), Carboxymethyl CS-sewage sludge biochar (CMC-SSBC), and magnetic sewage sludge biochar (MSSBC) were used for the adsorptive capturing of cationic and anionic metal ions such as  $Pb^{2+}$ ,  $Cd^{2+}$ ,  $Cu^{2+}$ ,  $Ag^+$ , and  $Cr_2O_7^{2-}$  in wastewater treatment (Iffhikar et al., 2020b, 2020a, 2018; Ngambia et al., 2019). Graphene, a two-dimensional carbon structure which has good chemical stability and higher theoretical surface area ( $\sim 2630 \text{ m}^2 \text{ g}^{-1}$ ) is considered as a good candidate for different applications including wastewater treatment (Zhang et al., 2020). Graphene oxide (GO) is well known derivative of graphene possessing oxygenated functional groups such as  $-COOH$ ,  $-OH$  and  $-O-$  groups, due to which it has found great attention as an effective adsorbing material for inorganic as well as organic contaminants (Li et al., 2021; Lv et al., 2018). Also, many researchers have reported the adsorbent composites of GO and CS for the capturing of heavy metals and different organic contaminants from water (Kovtun et al., 2020; Li et al., 2019). Recently, Sharma et al. (2019) reported grafting of CS with functionalized GO for selectively capturing of  $Pb^{2+}$  from aqueous solution over various heavy metals, e.g.,  $Pb^{2+}$ ,  $Cu^{2+}$ ,  $Ni^{2+}$ , and  $Cr^{3+}$  (Sharma et al., 2019).

Ethylenediaminetetraacetic acid is a very strong chelating agent for metal ions, and is easily ruined by catalysts (Lee et al., 2015). Presence of EDTA and GO in CS ultimately increases the metal ions capturing from the mixture of inorganic and organic contaminants due to its high number of functional groups. More recently, few studies have reported the use of EDTA as a functionalized material with GO or CS for the capturing of heavy metals (Croitoru et al., 2020; Shahzad et al., 2017; Zhang et al., 2016). More recently, our research group reported the trifunctional  $\beta$ -CD-EDTA-CS adsorbent in the simultaneous capturing of heavy metals and different organic pollutants from wastewater (Verma et al., 2022a).

Recently, our research group has synthesized GO-EDTA-CS via a chemical route for the capturing of both heavy metal ions (mercury (Hg (II)) and copper (Cu(II)) and organic dyes (methylene blue (MB) and crystal violet (CV)) from wastewater and reported its adsorption capacity of  $324 \pm 3.3$ ,  $130 \pm 2.8$ ,  $141 \pm 6.6$ , and  $121 \pm 3.5 \text{ mg g}^{-1}$  for Hg

(II), Cu(II), MB, and CV, respectively (Verma et al., 2022b). Inspired by this work, we are reporting the functionalization/grafting of CS polymer using EDTA and GO via one-pot chemical process to enhance the adsorption efficiency of CS for both heavy metals and commonly used drugs. The GO and EDTA moieties are bound to CS through the amide bond for the formation of GO-CS-EDTA adsorbent, in which each component possesses an important role in capturing the contaminants. Graphene oxide can capture both inorganic and organic contaminants because it has large negative charges on its surface and active functional groups. The EDTA component is responsible for both crosslinking in CS network as well as chelation with metal ions. CS moieties are the backbones of this new adsorbent, and their presence improves the yield of the adsorbing material. CS is a common material and used for the capturing of heavy metals, therefore, it is also considered to act as a supporting material for capturing the metal ions. Here, we chose cadmium ( $Cd^{2+}$ ) and lead ( $Pb^{2+}$ ) as inorganic contaminants, and ciprofloxacin (CIP) and sildenafil citrate (SDF) as organic contaminants to evaluate the adsorption performance of GO-CS-EDTA due to their commonly presence in wastewater. Firstly, pH effect on the adsorption efficiency of GO-CS-EDTA for each contaminant as well as kinetics and isotherms modelling were investigated in monocomponent systems. Then, simultaneous capturing of multiple heavy metals and organic contaminants at environmental levels was investigated. To the best of our knowledge, no one has reported this one-step functionalization process of CS for the simultaneous capturing of multiple metal ions and pharmaceutical drugs in water.

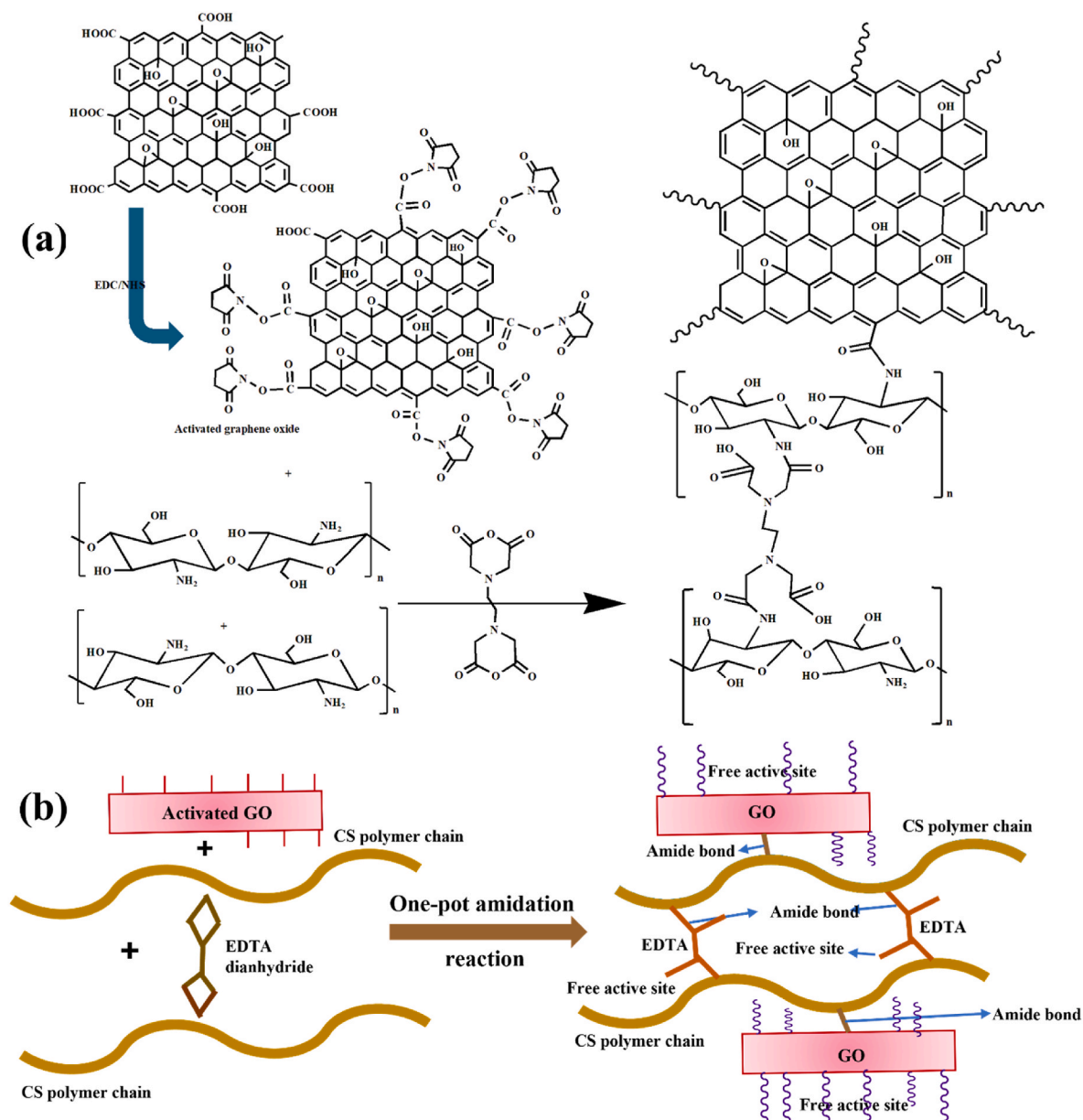
## 2. Experimental work

### 2.1. Materials

In this study, all the chemicals were used of analytical grade and used without any further purification. Chitosan flakes ( $\sim 85\%$  deacetylated) provided by Sigma-Aldrich (Seoul, Korea) had molecular weight of  $190000\text{--}375000 \text{ g mol}^{-1}$  and a viscosity of  $200\text{--}2000 \text{ MPa}$ . Graphite flakes (99% carbon based) with  $+200$  mesh size ( $\geq 70\%$ ) and EDTA were also purchased from Sigma-Aldrich (Seoul, Korea). Lead chloride ( $PbCl_2$ , 99.5%) and cadmium chloride hydrate ( $CdCl_2 \cdot xH_2O$ ,  $\geq 98\%$ ) were purchased from Samchun, (Deajeon, Korea). 1-ethyl-3-(3-dimethylaminopropyl) carbodiimide hydrochloride (EDC,  $\geq 97\%$ ), N-hydroxyl succinimide (NHS,  $\geq 98\%$ ), ciprofloxacin (CIP,  $\geq 98\%$ ) and sildenafil citrate (SDF,  $\geq 98\%$ ) were purchased from Sigma Aldrich (Seoul, Korea).

### 2.2. Grafting of CS polymer (GO-CS-EDTA)

Firstly, GO was synthesized using the previously reported modified Hummer's method (Hummers and Offeman, 1958; Verma et al., 2020). To improve the adsorption capacity of CS, grafting with GO and EDTA was carried out through the nucleophilic addition and elimination reactions (amide bond) between  $-COOH$  groups of GO and EDTA and the  $-NH_2$  groups of CS by the modified method (Chen et al., 2019b). The detailed procedure for the synthesis is as follows. Firstly, 5.0-g CS was dissolved in acetic acid solution (100 mL, 10%, v/v) at  $50^\circ \text{C}$ . Then, 5-time dilution was done with methanol. At the same time, 100-mg GO was suspended homogeneously in 50-mL DI water and activated by the addition of 0.1-M EDC and 0.1-M NHS. Then, 30-g EDTA dianhydride synthesized by the earlier reported method (Tülü and Geckeler, 1999; Verma et al., 2021a) was dispersed in 15-mL methanol and mixed in the CS methanol solution. Immediately, the activated GO solution was transferred to the EDTA-CS-methanol solution. Lastly, the mixture was stirred at room temperature for 24 h. The synthesized GO-CS-EDTA adsorbent was separated and washed sequentially with DI water and NaOH solution (pH 11) to remove extra EDTA. Subsequently, the adsorbent was washed again with DI water and 0.1-M HCl. Finally, the adsorbent was washed again with DI water followed by ethanol and dried at  $45^\circ \text{C}$  in a vacuum oven. After drying, the adsorbent was ground



**Scheme 1.** (a) Grafting of GO and EDTA on CS polymer for synthesis of GO–CS–EDTA adsorbent using EDTA as cross-linker in nucleophilic addition-elimination reactions; (b) Schematic diagram (~~~~ = amide bond and other part of GO).

with a mortar and pestle to harvest fine powder for future experiments.

### 2.3. Characterizations

The synthesized polymeric adsorbent was characterized to investigate the amorphous nature, morphology, surface area, thermal stability, etc. Details are given in the Supplementary information (Text S1).

### 2.4. Batch adsorption experiments

Stock solutions of inorganic ( $\text{Pb}^{2+}$ ,  $\text{Cd}^{2+}$ ) and other CIP and SDF contaminants were prepared and used for all experiments. Each adsorption experiment was performed by 25-mg adsorbent in 20-mL solution containing known amounts of contaminants in a shaking bath. The pH effect was examined with 100 mg  $\text{L}^{-1}$  and 25 mg  $\text{L}^{-1}$  initial concentrations of inorganic and organic contaminants in the pH range of 1.6–5.2 and 1.6–10.1, respectively. The pH was settled using 0.1 mol  $\text{L}^{-1}$   $\text{HNO}_3$  or NaOH solution for metal ions, and 0.1 mol  $\text{L}^{-1}$  HCl or NaOH

solution for organic contaminants, respectively.

For kinetics adsorption experiments, heavy metals (200 mg  $\text{L}^{-1}$ ) and organic contaminants (50 mg  $\text{L}^{-1}$ ) were used with time intervals range of 5–420 min. The initial concentrations effect on the capturing was investigated in 10–485 mg  $\text{L}^{-1}$  range for metal ions and 1–125 mg  $\text{L}^{-1}$  for organic contaminants. The adsorbent was separated after designated contact times using a syringe filter (0.45- $\mu\text{m}$  pore size). After diluted with 2.0%  $\text{HNO}_3$ , the initial and final concentrations of the metal ions were measured using Plasma atomic emission spectrometer (ICPE-9000, Shimadzu, Kyoto, Japan). The initial and final concentrations of organic contaminants were examined on ultra-high Liquid chromatograph-mass spectrometer (LCMS-8050, Shimadzu, Kyoto, Japan) through the multiple reaction monitoring (MRM) quantitation. All the adsorption tests were conducted three times and the average values were chosen to calculate the adsorption efficiency (%) and adsorption capacity (mg  $\text{g}^{-1}$ ) of the adsorbent from the following equations, respectively:

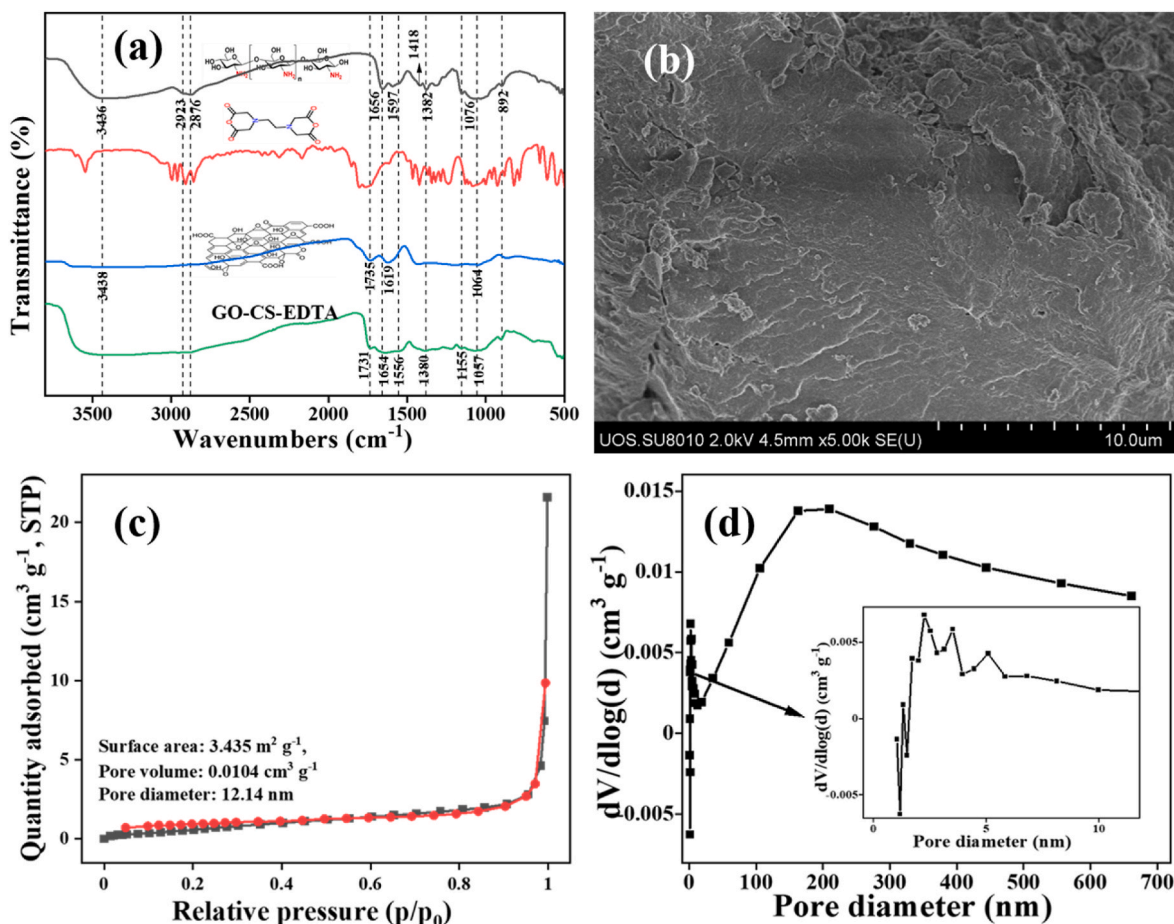


Fig. 1. (a) FTIR spectra, (b) FESEM image (c)  $N_2$  adsorption-desorption and, (d) pore size distribution of the synthesized GO–CS–EDTA adsorbent.

$$\text{Removal efficiency (\%)} = \left( \frac{C_0 - C_e}{C_0} \right) \times 100 \quad (1)$$

$$\text{Adsorption capacity (} q_e \text{)} = (C_0 - C_e) \times \frac{V}{m} \quad (2)$$

where  $C_0$  and  $C_e$  are in  $\text{mg g}^{-1}$  initial and equilibrium concentrations, respectively.  $V$  (L) and  $m$  (g) are the volume of polluted solution and mass of the adsorbent, respectively.

The adsorption performance of the synthesized GO–CS–EDTA was also investigated with the mixture of both heavy metals and organic contaminants at environmental levels ( $\mu\text{g L}^{-1}$  to  $\text{mg L}^{-1}$ ) in real wastewater. The real wastewater was collected from the Jungnang Water Reclamation Center, Seoul, Korea. All the experiments were performed at 18–20 °C temperature.

### 3. Results and discussions

#### 3.1. Characterizations of GO–CS–EDTA

Scheme 1 represents the grafting of GO and EDTA on CS for the synthesis of GO–CS–EDTA in which EDTA works as a crosslinking agent between CS chains and GO as a supporting component for capturing both heavy metals and organic contaminants. In the formation of grafted polymer, carboxylic acids of both GO and EDTA reacted with the primary amine of CS via the nucleophilic addition-elimination reaction to obtain the amide formation, as occurred in succinic anhydride (R. K. Bansal, 2012).

The FT-IR spectra of the raw materials, CS, EDTA dianhydride, GO and synthesized GO–CS–EDTA polymer adsorbent are displayed in

Fig. 1 (a). The CS shows a broad peak situated at  $3436 \text{ cm}^{-1}$  due to overlapping of hydroxyl and amine (O–H and N–H) stretching vibrations, while peaks situated at  $2923$  and  $2876 \text{ cm}^{-1}$  are ascribed to stretching of asymmetric and symmetric C–H groups, respectively. Peaks occurring at  $1656$  and  $1597 \text{ cm}^{-1}$  would be due to C=O stretching vibrations of NHCO– and N–H deformation of amine groups, respectively. The peaks situated at  $1154 \text{ cm}^{-1}$  occurred due to asymmetric vibrations of C–O. Lastly, the peaks situated at  $1076 \text{ cm}^{-1}$  and  $892 \text{ cm}^{-1}$  occurred due to skeletal stretching to C–O–C confirming the polysaccharide structure of CS (Chandra et al., 2015; Perumal et al., 2019). In the GO, FT-IR peaks existed at  $3438$  and  $1735 \text{ cm}^{-1}$  would be corresponding to –OH groups and C=O stretching vibrations of the COOH groups, respectively. The peaks observed at  $1619$ ,  $1434$  and  $1064 \text{ cm}^{-1}$  were corresponding to C=C stretching mode of the  $\text{sp}^2$  carbon skeletons, C–OH, and C–O–C, respectively. These GO peaks confirm the conversion of graphite flakes into GO by the modified Hummer’s method. In the case of GO–CS–EDTA formation, two new vibration peaks were assigned at  $1654$  and  $1731 \text{ cm}^{-1}$ , which are corresponding to the C=O stretching vibrations of amide bond and –COOH groups introduction, respectively. These peaks ascribed the formation of amide bond of CS with EDTA dianhydride and activated GO. Therefore, these results confirmed the proper grafting of GO and EDTA on CS. FESEM was applied to investigate the morphology of the GO–CS–EDTA polymer and its result is displayed in Fig. 1 (b). It can be seen a thin layer with porous and rough structures from the figure, which confirms the grafting of GO on the EDTA–CS polymer material. The elemental mapping and EDS spectrum are shown in Fig. 1S (Supplementary information) which confirm the elemental distribution and their compositions over the surface. Elemental distribution of C, N, and O elements clearly indicates the uniform distribution throughout the surface, and their atomic

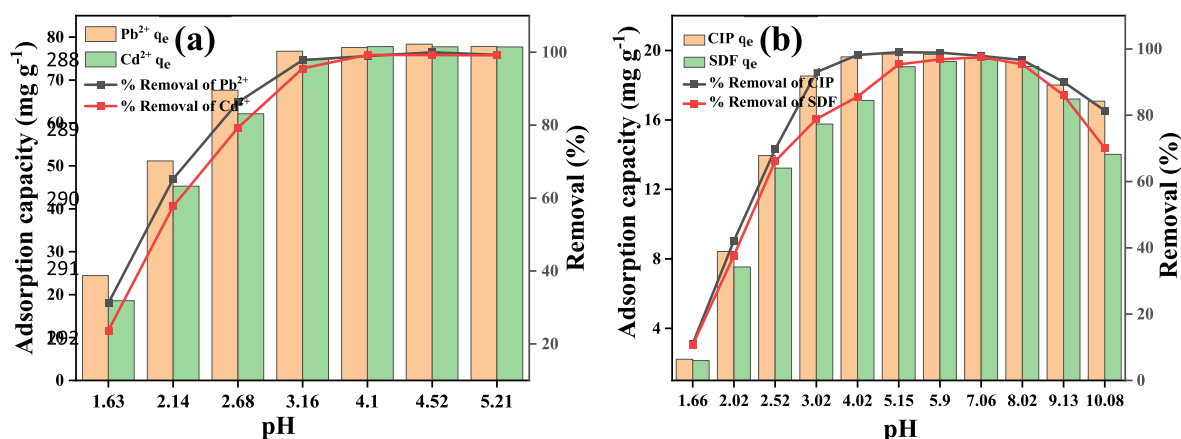


Fig. 2. Effect of pH on the removal efficiency and adsorption capacity of GO–CS–EDTA for (a) Pb<sup>2+</sup> and Cd<sup>2+</sup> and (b) CIP and SDF contaminants.

compositions (C = 59.9%, N = 18.5% and O = 21.6%) confirmed the presence of abundant elements, which were consistent with our expectation. N<sub>2</sub> adsorption-desorption isotherm and BJH pore size distribution of the prepared GO–CS–EDTA adsorbent are shown in Fig. 1 (c) and (d), respectively. The multipoint BET surface area, cumulative pore volume and average pore diameter were found to be 3.435 m<sup>2</sup> g<sup>-1</sup>, 0.0104 cm<sup>3</sup> g<sup>-1</sup> and 12.14 nm, respectively. Interestingly, the pore size distribution showed a porosity in the range of 162–276 nm, which was attributed to the crosslinking in the adsorbent. Similar to other previously reported polymers, GO–CS–EDTA did not have higher surface area or porosity. Nonetheless, it shows an excellent removal efficiency for both inorganic and organic contaminants. The reason might be attributed to the availability of the large number of active functional groups on the synthesized polymeric adsorbent (Qin et al., 2019).

Fig. 2S (a) indicates the powder XRD patterns of monocomponent-containing adsorbents and the synthesized GO–CS–EDTA adsorbent. The CS exhibited two wide peaks situated at 9.42° and 19.87° which confirmed the amorphous nature of used CS. Graphene oxide shows a peak situated at 2θ = 10.12°, confirming the formation of GO from graphite flakes. In comparison to CS and GO, the XRD pattern of GO–CS–EDTA did not show peaks of CS and GO but a new broad and weak peak situated at 22.23°, which confirmed the chemical reaction of CS with GO and EDTA dianhydride to form the amide bond (–NHCO–). This new broad and wide peak confirmed the amorphous and polymer nature of the synthesized adsorbent. Fig. 2S (b) displays the TGA and DTG curve of used GO–CS–EDTA polymer. TGA provides three weight losses in the range of 35–110, 185–315, and 345–610 °C. These weight losses were due to water loss, EDTA decomposition, and chitosan decomposition, respectively. Also, DTG curve clearly indicates the three-

pyrolysis processes which are situated at 70, 230 and 278 °C.

### 3.2. Effect of pH

Solution pH is an important parameter in the water contaminants capturing due to changing in the surface charge of an adsorbent, competition between hydrogen ions and contaminants, and degree of ionization and solubility of the contaminants. Fig. 2 (a) and (b) display the effect of pH on the removal efficiency and adsorption capacity of the synthesized adsorbent for metal ions and organic contaminants in the range of pH 1.6–5.2 and pH 1.6–10.1, respectively. The alkaline solution for the heavy-metal capturing was not investigated since metal hydroxides form precipitates at a higher pH (Visual MINTEQ ver. 3.0). Data indicates that as the solution pH increases, the removal efficiencies of metal ions increased rapidly to > 98% above pH 2.9 and then very slowly to attain the dynamic equilibrium. The maximum adsorption capacity was achieved above pH 3 for both Pb<sup>2+</sup> and Cd<sup>2+</sup>. This behavior can be described from the view point of the zero charge (pH<sub>zpc</sub>) of the GO–CS–EDTA adsorbent which was calculated from pH drift process (Verma et al., 2017), and found to be 2.92 (Fig. 3S). When the solution pH was lower than pH<sub>zpc</sub>, the surface of the adsorbent became positive, which would get electrostatic repulsion against positively charged metal ions and negatively affect the removal efficiency. As the pH increased above 2.92, on the other hand, the surface became negatively charged and the electrostatic repulsion could be reduced, which would enhance the electrostatic attraction between the adsorbent and metal ions, resulting in higher removal efficiency. Moreover, at a lower pH, the hydrophilic functionalities in the form of –OH, –COOH, and –NH<sub>2</sub> groups on the surface of the GO–CS–EDTA became positively charged

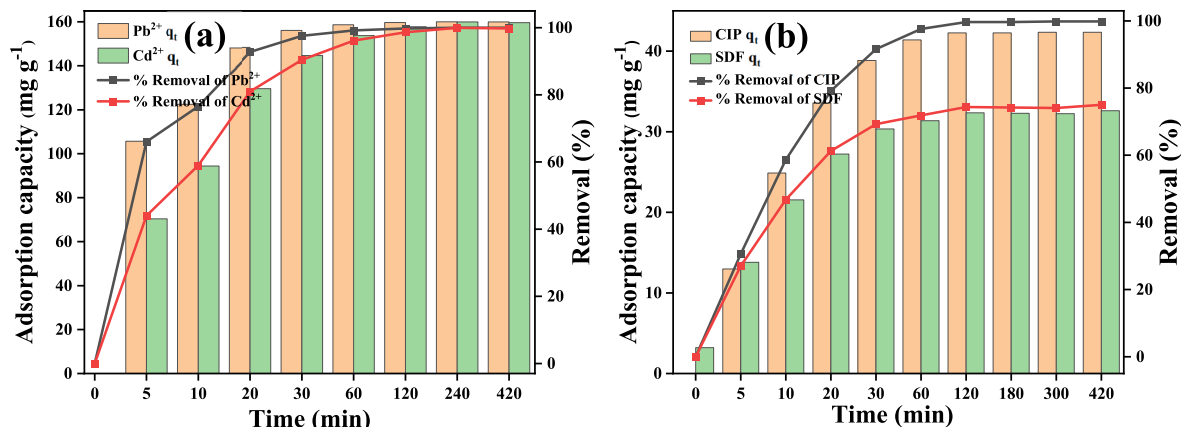


Fig. 3. Effect of contact time on the removal efficiency and adsorption capacity by GO–CS–EDTA adsorbent, (a) Pb and Cd ions, and (b) CIP and SDF contaminants.

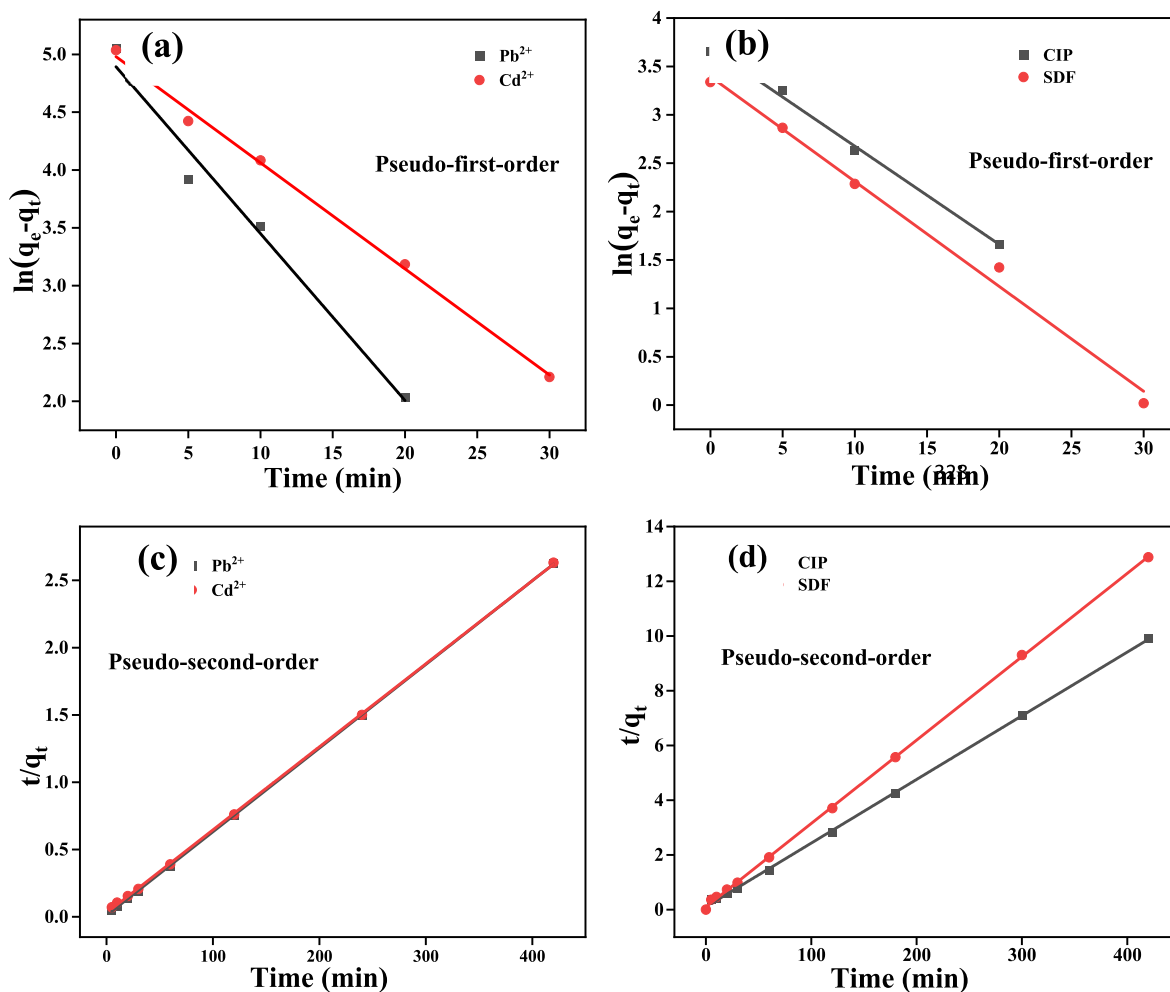


Fig. 4. PFO linear plots for (a)  $\text{Pb}^{2+}$  and  $\text{Cd}^{2+}$  ions, (b) CIP and SDF, and PSO linear plots for (c)  $\text{Pb}^{2+}$  and  $\text{Cd}^{2+}$  ions, and (d) CIP and SDF onto GO–CS–EDTA polymer.

due to protonation and the bonding could be made weaker due to the increased electrostatic repulsion. By increasing pH, the positive charge of the surface became weaker and an electrostatic interaction between the metal ions and the surface would occur (Cui et al., 2015). On the other hand, the removal efficiency of organic contaminants (i.e., CIP and SDF) was observed different from those of metal ions. The removal efficiencies were observed increasing with the increase of pH from 1.5 to 4–5 and then, showing a plateau curve in the range of 4–6 and 5–8, respectively. This adsorption behaviors of CIP and SDF can be explained with water pH and speciation nature of CIP and SDF. As the water pH not only affects the adsorbent surface charge but also the speciation of CIP and SDF. The CIP and SDF possess two  $\text{pK}_{\text{a}}$  values;  $\text{pK}_{\text{a}1}$  and  $\text{pK}_{\text{a}2}$  of CIP and SDF are 6.1 and 8.7, and 8.7 and 9.7, respectively. These contaminants can be positively charged at pH less than  $\text{pK}_{\text{a}1}$ , while negatively charged at pH above  $\text{pK}_{\text{a}2}$ . Thereby, when the solution pH exceeds 8.7 and 9.7, the interaction between the negatively charged GO–CS–EDTA and contaminants becomes weaker, resulting in less adsorption.

### 3.3. Adsorption kinetics

The effects of contact time on the removal efficiency and adsorption capacity of GO–CS–EDTA for each contaminant were investigated and displayed in Fig. 3. As indicated in the figure, the adsorption rate was very fast in the initial 5 min, so we could attain 66, 44, 30.61, and 27.04% removal efficiencies for the  $\text{Pb}^{2+}$ ,  $\text{Cd}^{2+}$ , CIP and SDF, respectively. During this time of period, adsorption capacities were found to be 105.68, 70.40, 12.98 and 13.8  $\text{mg g}^{-1}$  for  $\text{Pb}^{2+}$ ,  $\text{Cd}^{2+}$ , CIP and SDF, respectively, which are sufficiently high for the purpose of water treatment. Among them, metal ions attained the equilibrium in 30–60 min while organic contaminants did it in 120–180 min. Therefore, 4 h was decided as the equilibrium contact time for the further experiments. Moreover, the adsorption kinetics mechanism was analyzed using pseudo-first-order (PFO) and pseudo-second-order (PSO) kinetics models as given in Text 2S.

The linear fits made on the PFO and PSO kinetics models are shown

Table 1

Model parameters of PFO and PSO kinetics for adsorption of metal ions and organic contaminants onto GO–CS–EDTA adsorbent.

System	PFO				PSO		
	$q_{\text{e,exp}}$ ( $\text{mg g}^{-1}$ )	$q_{\text{e,cal}}$ ( $\text{mg g}^{-1}$ )	$k_1$ ( $\text{min}^{-1}$ )	$R^2$	$q_{\text{e,cal}}$ ( $\text{mg g}^{-1}$ )	$k_2$ ( $\text{g mg}^{-1} \text{min}^{-1}$ )	$R^2$
$\text{Pb}^{2+}$	156.49	159.98	0.144	0.979	160.77	0.0086	0.999
$\text{Cd}^{2+}$	152.78	159.62	0.091	0.988	160.25	0.0041	0.999
CIP	42.33	40.04	0.108	0.986	43.12	0.0038	0.999
SDF	32.60	29.66	0.101	0.988	32.89	0.0028	0.999

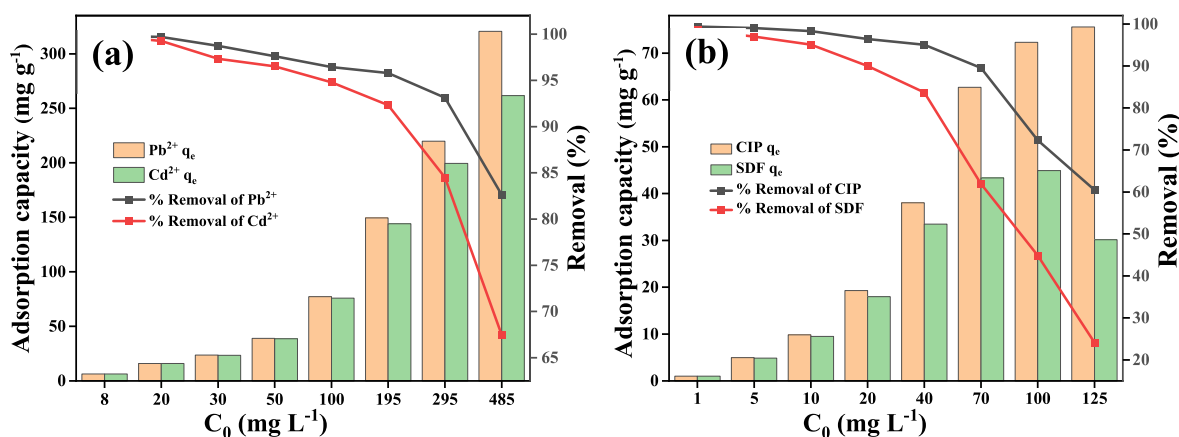


Fig. 5. Effect of initial concentrations on the removal efficiency and adsorption capacity of GO–CS–EDTA adsorbent for (a) Pb<sup>2+</sup> and Cd<sup>2+</sup> ions, and (b) CIP and SDF contaminants.

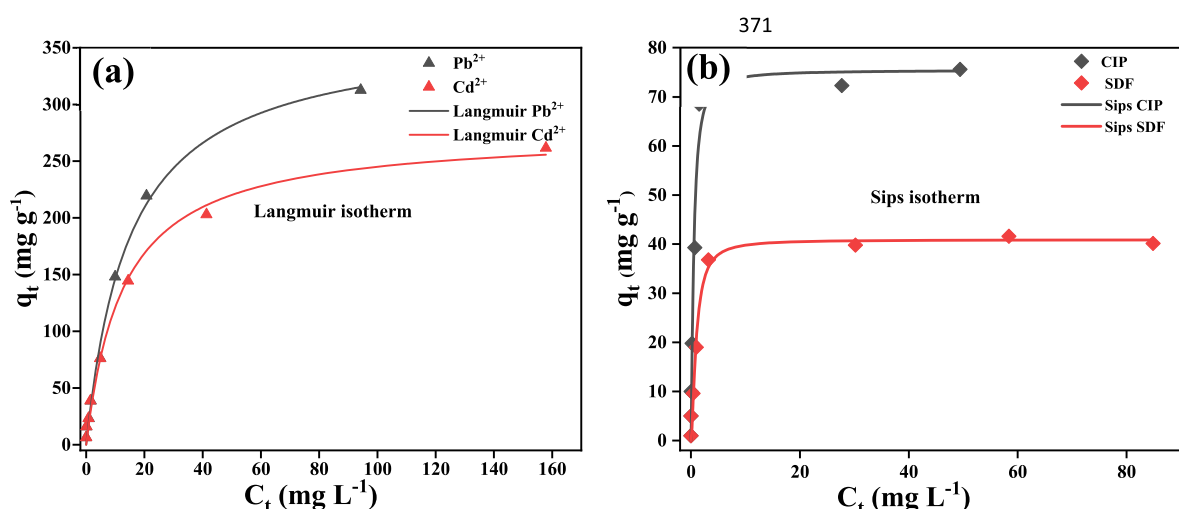


Fig. 6. (a) Langmuir isotherm for Pb<sup>2+</sup> and Cd<sup>2+</sup> ions and (b) Sips isotherm for CIP and SDF onto GO–CS–EDTA adsorbent.

in Fig. 4, and all the kinetics parameter values are listed in Table 1. A higher correlation coefficient value ( $R^2 > 0.999$ ) and a better agreement between the calculated  $q_e$  ( $q_{e,cal}$ ) and experimental  $q_e$  ( $q_{e,exp}$ ) could be observed from the PSO kinetic model than PFO. The perfect fits of the PSO kinetics model to the experimental data from the GO–CS–EDTA adsorption experiments with metal ions or organic contaminants confirmed that the chemisorption would be the controlling step for the adsorption of both metal ions and organic contaminants on GO–CS–EDTA. It was also noticed that Pb<sup>2+</sup> and Cd<sup>2+</sup> had a faster adsorption behavior (higher  $k_2$  values for metal ions as shown in Table 1) than the CIP and SDF. This faster adsorption rates for the metal ions might be due to the larger availability of adsorption sites created by EDTA for metal ions in comparison to organic contaminants (Repo et al., 2013).

### 3.4. Adsorption isotherm

Fig. 5 displays the effect of initial concentrations on the removal efficiency and adsorption capacity of the GO–CS–EDTA polymer adsorbent for the heavy metal ions and organic contaminants. As exhibited in the figure, the removal efficiencies decrease, while adsorption capacities were enhanced continuously with the concentration increasing. This increment in the capacity was due to the availability of large numbers of active sites on the adsorbent which interacts with opposite charged contaminants and higher driving force for mass

Table 2  
Adsorption isotherms parameters for metals and organic contaminants onto GO–CS–EDTA adsorbent.

Isotherms Models	Parameters	Contaminants			
		Pb <sup>2+</sup>	Cd <sup>2+</sup>	CIP	SDF
Langmuir model	$q_{m,exp}$ (mg g <sup>-1</sup> )	349.20	261.70	75.60	40.10
	$q_{m,cal}$ (mg g <sup>-1</sup> )	351.20	264.10	76.80	42.10
	$K_L$ (L mg <sup>-1</sup> )	0.067	0.078	1.470	0.978
	$R^2$	0.997	0.994	0.973	0.981
Freundlich model	$K_F$	44.11	42.46	41.85	24.74
	$n$	2.413	2.924	5.930	6.033
	$R^2$	0.953	0.966	0.880	0.891
Sips model	$q_m$ (mg g <sup>-1</sup> )	354.50	290.10	75.40	40.90
	$K_S$ (L mg <sup>-1</sup> )	0.072	0.055	2.001	1.029
	$n_S$	0.937	1.276	0.750	0.650
	$R^2$	0.992	0.991	0.987	0.983

transfer (Gomes et al., 2013; Usman et al., 2021).

To describe the relationship between the initial contaminant concentrations and equilibrium adsorption capacity of the adsorbent, three important isotherms models, i.e., Langmuir, Freundlich and Sips models were applied. Details are given in Text 3S. Fig. 6 and Fig. 4S display the non-linear fits of Langmuir, Freundlich, and Sips models to experimental data and Table 2 summarizes all the regression parameters for the target

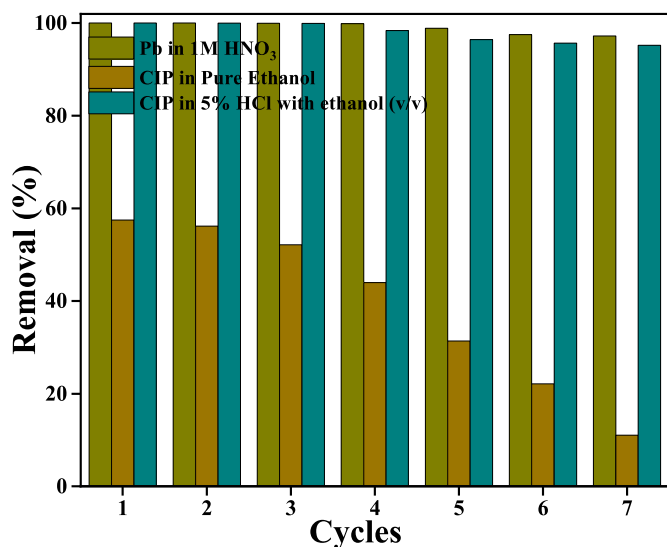


Fig. 7. Removal efficiency during reusability of GO–CS–EDTA polymer for  $Pb^{2+}$  and CIP contaminants.

metal ions and organic contaminants.

Data clearly indicates that the Langmuir would be the best isotherm model for metal ions in comparison to the Freundlich and Sips models; higher correlation values ( $R^2$ ) could be obtained using the Langmuir model than the Freundlich and Sips ones. Also, the experimental values were closer to the calculated ones obtained by the Langmuir model as shown in Table 2, which confirms the uniform distribution of active sites on the adsorbent possibly due to the EDTA group of GO–CS–EDTA for  $Pb^{2+}$  and  $Cd^{2+}$ . Conversely, the adsorption of organic contaminants to the adsorbent was better illustrated by the Sips model than the Langmuir or the Freundlich (Fig. 6); a better  $R^2$  values (0.983–0.987) could be obtained by the Sips model. The experimental values were also closer with calculated  $q_m$  values acquired by Sips model, confirming the presence of heterogeneously active sites such as EDTA and GO for the adsorption of CIP and SDF (Delgado et al., 2019; Yu et al., 2016). The capturing of organic contaminants can be attributed to electrostatic interactions between the cationic contaminant species with phenol group, carboxyl group, C–C, C–O,  $\pi$ – $\pi$  C=N, etc. of GO, EDTA and CS (Chen et al., 2015; Karimi-Maleh et al., 2021; Zhao et al., 2017). Interestingly, CIP displayed a higher adsorption capacity than SDF, probably due to more interactions between the CIP with GO–CS–EDTA caused by the fluorine group of CIP which has a strong electron-withdrawing ability (Fig. 5S and Table 1S).

In Table 2S, the adsorption performance of synthesized GO–CS–EDTA adsorbent was compared with those of other reported adsorbents based on CS and GO for the capturing of  $Pb(II)$ ,  $Cd(II)$ , CIP and SIP contaminants. Obviously, GO–CS–EDTA displayed an excellent adsorption capacity for the capturing of both inorganic and organic contaminants, which confirms that the currently synthesized adsorbent is an effective and alternative adsorbent for the capturing of single class pollutants as well as mixed contaminants in wastewater.

### 3.5. Reusability

The reusability and stability are another two important parameters of an adsorbent for practical uses. Therefore, inorganic ( $Pb^{2+}$ ) and organic (CIP) contaminants were used to examine the reusability of GO–CS–EDTA. For the purpose, the adsorbent was regenerated using 1.0-M  $HNO_3$ , pure ethanol and 5% HCl in ethanol (v/v) after each adsorption cycle, following the previous reports on regenerating adsorbents loaded with metal and organic contaminants (Repo et al., 2010; Usman et al., 2021). Fig. 7 and Fig. 6S display the removal efficiencies

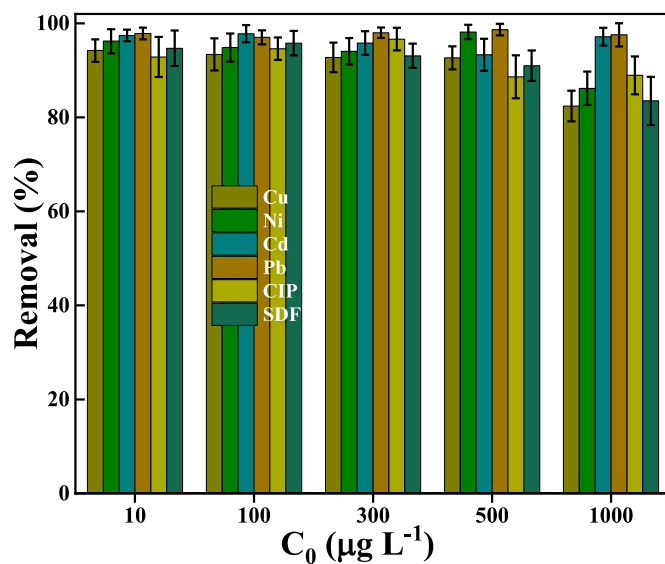


Fig. 8. Adsorption performance of GO–CS–EDTA for simultaneous capturing of multiple heavy metals and organic contaminants at different environmental levels from real wastewater.

and the adsorption capacities of the synthesized adsorbent for seven continuous cycles. Data clearly shows the insignificant decrement in removal efficiency for  $Pb^{2+}$  even after seven continuous adsorption-desorption cycles (only 3%). In the case of CIP, when pure ethanol was used alone for regeneration, the reusability of the adsorbent became very low ( $\leq 57\%$ ) even after the first cycle; it decreased down to 11% after seventh cycle. When GO–CS–EDTA was regenerated by 5% HCl in ethanol (v/v), however, almost complete removal efficiency could be maintained for the first three cycles and the efficiency decreased slightly (only 5%) even after seven consecutive adsorption-desorption cycles. These results imply that GO–CS–EDTA has a potential to be regenerated and reused still to show a stable removal performance.

### 3.6. Simultaneous capturing of mixed inorganic and organic contaminants at environmental level from real secondary effluent

The synthesized material was applied to capture the organic and inorganic contaminants at an environmental level in the secondary effluent collected from Jungnang Water Reclamation Center, Seoul, South Korea. The different physicochemical properties of this wastewater are listed in. The pH was 6.80 of wastewater which was adjusted to 5.10 by 0.1 M HCl solution before treating with adsorbent. The mixture of  $Cu^{2+}$ ,  $Ni^{2+}$ ,  $Cd^{2+}$ ,  $Pb^{2+}$ , CIP and SDF contaminants was spiked in the wastewater in the range of 1–1000  $\mu g L^{-1}$ , which covers the contaminants levels often occurring in water environment (Schwarzenbach et al., 2006). The experiment was performed by mixing 100-mg adsorbent in 100-mL wastewater. The results showed that more than 83% of both inorganic and organic contaminants could be adsorbed by the GO–CS–EDTA adsorbent (Fig. 8). The small loss in the efficiency probably due to existence of other chemicals and biological entities in the medium. Overall, the result clearly demonstrates that GO–CS–EDTA can simultaneously and successfully remove both heavy metal ions and organic contaminants at environment-relevant levels from wastewater. Therefore, it can be assumed that GO–CS–EDTA is a promising adsorbent that can simultaneously remove a wide range of inorganic and organic contaminants from wastewater.

### 3.7. Proposed adsorption mechanism

Figs. 7S and 8S display the elemental distribution of existing

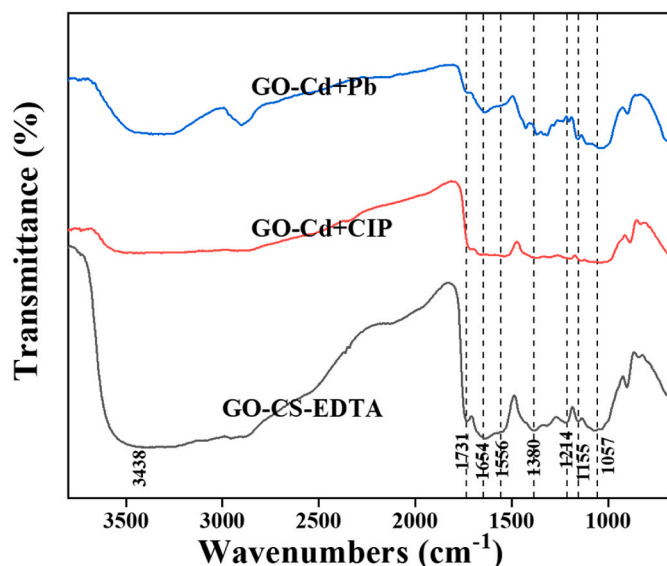


**Fig. 9.** FTIR spectra of GO–CS–EDTA before and after adsorption of mixture of inorganic and organic ( $\text{Cd}^{2+}$  and CIP) or inorganic ( $\text{Pb}^{2+}$  and  $\text{Cd}^{2+}$ ) contaminants.

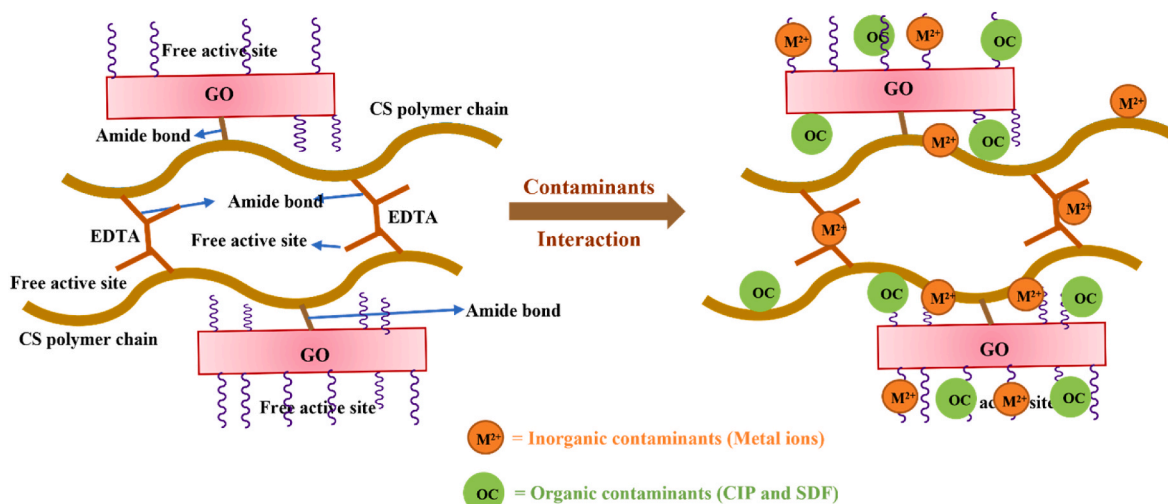
elements in GO–CS–EDTA after simultaneous capturing of inorganic and organic ( $\text{Cd}^{2+}$  and CIP), and inorganic ( $\text{Pb}^{2+}$  and  $\text{Cd}^{2+}$ ) contaminants from aqueous solution, respectively.  $\text{Cd}^{2+}$  and  $\text{F}^-$  were uniformly distributed throughout the whole surface of GO–CS–EDTA, which indicates the profitable loading of metal ions ( $\text{Cd}^{2+}$ ) and CIP (F is from CIP). This well distribution of  $\text{Cd}^{2+}$  and CIP over the surface of the GO–CS–EDTA presented in Fig. 7S confirms the well distributed sites for adsorption. Also, higher amount of  $\text{Cd}^{2+}$  on the surface of GO–CS–EDTA was observed than CIP as clearly observed by elemental mapping, which is also in a strong agreement with adsorption isotherm capacity findings. Interestingly, it is observed that the fluorine distribution (CIP) is corresponding to spots for carbon, nitrogen and oxygen which indicate the interaction of CIP with the amine group of CS and the carboxylic or phenolic groups of GO. A similar type of interaction between organic contaminants with CS or GO was reported in the literature (Alnajrani and Alsager, 2020; Chen et al., 2015; S. J. Ma et al., 2017). FT-IR spectra of GO–CS–EDTA were also investigated to further confirm the adsorption and the related mechanism after the adsorption of a mixture of inorganic and organic ( $\text{Cd}^{2+}$  and CIP) or inorganic ( $\text{Pb}^{2+}$

and  $\text{Cd}^{2+}$ ) contaminants by the adsorbent (Fig. 9). The peaks observed due to the presence of hydroxyl ( $-\text{OH}$ ) and amine ( $-\text{NH}_2$ ) groups ( $3425\text{--}3267\text{ cm}^{-1}$ ) in the GO–CS–EDTA adsorbent became wider and broader ( $3520\text{--}3159\text{ cm}^{-1}$ ) after simultaneous adsorption of  $\text{Cd}^{2+}$  and CIP. This might be probably due to hydrogen bonds between CIP (fluorine) and the hydroxyl groups of the adsorbent. In the case of heavy metals adsorption, a significant decrement in the intensity of hydroxy and amine groups ( $3425\text{--}3267\text{ cm}^{-1}$ ) and the carboxylic group ( $1734\text{ cm}^{-1}$ ) could be observed, confirming the interaction of heavy metals with existing groups ( $-\text{COOH}$  and  $-\text{OH}$ ) on the adsorbent. Similar types of behaviors were also observed in the earlier reported literature (Cui et al., 2015; Liu et al., 2019; J. S. Ma et al., 2017).

Thus, based on the elemental mapping, adsorption isotherms, and FT-IR analysis, a probable mechanism for the adsorption of the targeted inorganic and organic contaminants is represented in Scheme 2. The reason behind the best adsorption capacity of GO–CS–EDTA might be: (a) EDTA, a well-known hexavalent ligand possesses dual nature in the adsorbent as a crosslinking agent for the CS polymer and a complexing agent for inorganic contaminants (heavy metals). Also, EDTA–dianhydride produces hydrogel and two acidic sites through inter or intra molecular crosslinking reactions with CS polymer chains. Apart from it, the active functional groups of GO (especially  $-\text{OH}$ ) interact with heavy metals as observed in FT-IR data. (b) The existing active functional groups on GO–CS–EDTA also simultaneously interact with organic contaminants. Therefore, all moieties of the synthesized adsorbent play an important role in the adsorptive capturing of organic and inorganic contaminants via electrostatic interactions and complexation reactions.

#### 4. Conclusions

In summary, functionalization of CS was carried out to prepare the GO–CS–EDTA adsorbent, which was characterized using FTIR, FESEM, EDS, BET, XRD, and TGA. This adsorbent demonstrated excellent monolayer adsorption capacities of  $351.20$  and  $264.10\text{ mg g}^{-1}$  for  $\text{Pb}^{2+}$  and  $\text{Cd}^{2+}$ , respectively, while heterogeneous sorption capacities of  $75.40$  and  $40.90\text{ mg g}^{-1}$  for CIP and SDF, respectively, due to the coordination property of EDTA and electrostatic interactions with functional groups of GO. Adsorption and characterization experiments confirmed the role of each moiety existing in GO–CS–EDTA: CS plays as a backbone of the polymer chain, EDTA behaves as a crosslinker and complexing agent for adsorption of metal ions and GO works as a supportive site for both inorganic and organic contaminants. The kinetics results followed the PSO model and showed faster adsorption of inorganic contaminants to the adsorbent than organic contaminants due to



**Scheme 2.** Adsorption mechanism of heavy metal ions and organic contaminants towards GO–CS–EDTA polymer.

electrostatic interactions caused by charged functional groups available on EDTA. The synthesized adsorbent exhibited an excellent reusability even after seven adsorption-desorption cycles towards both types of contaminants, which would minimize the cost of applying the adsorbent. At last, the adsorbent showed an excellent performance when it was applied for simultaneous capturing multiple inorganic and organic contaminants at environment-relevant levels in real secondary effluent wastewater; more than 80% removal efficiency could be obtained.

### Credit author statement

Monu Verma: Conceptualization, Methodology, Investigation, Writing – original draft; Ashwani Kumar: Investigation; Ingyu Lee, Vinod Kumar: Review of Writing; Ju-Hyun Park, Hyunook Kim: Conceptualization, Supervision, Writing – review & editing.

### Declaration of competing interest

The authors declare that they have no known competing financial interests or personal relationships that could have appeared to influence the work reported in this paper.

### Acknowledgements

Monu Verma thanks to NRF Korea for providing funding BP Program (2019H1D3A1A01102657). Ju-Hyun Park was supported by a grant from the National Institute of Environment Research (NIER), funded by the Ministry of Environment (MOE) of the Republic of Korea (NIER-2021-01-01-042). Hyunook Kim is funded by the Korea Environment Industry & Technology Institute (KEITI) through the Post Plastic, a specialized program of the Graduate School funded by the Korea Ministry of Environment (MOE). This paper has been also supported by the RUDN University Strategic Academic Leadership Program.

### Appendix A. Supplementary data

Supplementary data to this article can be found online at <https://doi.org/10.1016/j.envpol.2022.119130>.

### References

- Ajiboye, T.O., Oyewo, O.A., Onwudiwe, D.C., 2021. Simultaneous removal of organics and heavy metals from industrial wastewater: a review. *Chemosphere* 262, 128379. <https://doi.org/10.1016/j.chemosphere.2020.128379>.
- Alnajrani, M.N., Alsager, O.A., 2020. Removal of antibiotics from water by polymer of intrinsic microporosity: isotherms, kinetics, thermodynamics, and adsorption mechanism. *Sci. Rep.* 10, 1–14. <https://doi.org/10.1038/s41598-020-57616-4>.
- Bansal, R.K., 2012. *Organic Reaction Mechanisms*. New Academic Science.
- Chandra, S., Chakraborty, N., Dasgupta, A., Sarkar, J., Panda, K., Acharya, K., 2015. Chitosan nanoparticles: a positive modulator of innate immune responses in plants. *Sci. Rep.* 5, 1–14. <https://doi.org/10.1038/srep15195>.
- Chen, H., Gao, B., Li, H., 2015. Removal of sulfamethoxazole and ciprofloxacin from aqueous solutions by graphene oxide. *J. Hazard Mater.* 282, 201–207. <https://doi.org/10.1016/j.jhazmat.2014.03.063>.
- Chen, B., Chen, S., Zhao, H., Liu, Y., Long, F., Pan, X., 2019a. A versatile  $\beta$ -cyclodextrin and polyethyleneimine bi-functionalized magnetic nano-adsorbent for simultaneous capture of methyl orange and Pb(II) from complex wastewater. *Chemosphere* 216, 605–616. <https://doi.org/10.1016/j.chemosphere.2018.10.157>.
- Chen, B., Zhao, H., Chen, S., Long, F., Huang, B., Yang, B., Pan, X., 2019b. A magnetically recyclable chitosan composite adsorbent functionalized with EDTA for simultaneous capture of anionic dye and heavy metals in complex wastewater. *Chem. Eng. J.* 356, 69–80. <https://doi.org/10.1016/j.cej.2018.08.222>.
- Cho, C.W., Lim, C.R., Cho, B.G., Mun, S.B., Choi, J.W., Zhao, Y., Kim, S., Yun, Y.S., 2021. Development of prediction models for adsorption properties of chitin and chitosan for micropollutants. *Chem. Eng. J.* 426, 131341. <https://doi.org/10.1016/j.cej.2021.131341>.
- Croitoru, A., Ficai, A., Ficai, D., Trusca, R., Dolet, G., Andronesco, E., Turculeț, S.C., 2020. Chitosan/graphene oxide nanocomposite water purification. *Materials* 13, 1–13.
- Cui, L., Wang, Y., Gao, L., Hu, L., Yan, L., Wei, Q., Du, B., 2015. EDTA functionalized magnetic graphene oxide for removal of Pb(II), Hg(II) and Cu(II) in water treatment: adsorption mechanism and separation property. *Chem. Eng. J.* 281, 1–10. <https://doi.org/10.1016/j.cej.2015.06.043>.

- Delgado, N., Capparelli, A., Navarro, A., Marino, D., 2019. Pharmaceutical emerging pollutants removal from water using powdered activated carbon: study of kinetics and adsorption equilibrium. *J. Environ. Manag.* 236, 301–308. <https://doi.org/10.1016/j.jenvman.2019.01.116>.
- Gomes, E.C.C., Sousa, A.F. De, Vasconcelos, P.H.M., Melo, D.Q., Diógenes, I.C.N., Sousa, E.H.S. De, Ronaldo, F., San, R.A.S., Longhinotti, E., 2013. Synthesis of bifunctional mesoporous silica spheres as potential adsorbent for ions in solution. *Chem. Eng. J.* 214, 27–33. <https://doi.org/10.1016/j.cej.2012.10.053>.
- Guo, D.M., An, Q., Da, Xiao, Z.Y., Zhai, S.R., Yang, D.J., 2018. Efficient removal of Pb(II), Cr(VI) and organic dyes by polydopamine modified chitosan aerogels. *Carbohydr. Polym.* 202, 306–314. <https://doi.org/10.1016/j.carbpol.2018.08.140>.
- Hu, X., Xu, G., Zhang, H., Li, M., Tu, Y., Xie, X., Zhu, Y., Jiang, L., Zhu, X., Ji, X., Li, Y., Li, A., 2020. Multifunctional  $\beta$ -cyclodextrin polymer for simultaneous removal of natural organic matter and organic micropollutants and detrimental microorganisms from water. *ACS Appl. Mater. Interfaces* 12, 12165–12175. <https://doi.org/10.1021/acsami.0c00597>.
- Hummers, W.S., Offeman, R.E., 1958. Preparation of graphitic oxide. *J. Am. Chem. Soc.* 80, 1339. <https://doi.org/10.1021/ja01539a017>.
- Iftthikar, J., Wang, T., Khan, A., Jawad, A., Sun, T., Jiao, X., Chen, Z., Wang, J., Wang, Q., Wang, H., Jawad, A., 2017. Highly efficient lead distribution by magnetic sewage sludge biochar: sorption mechanisms and bench applications. *Bioresour. Technol.* 238, 399–406. <https://doi.org/10.1016/j.biortech.2017.03.133>.
- Iftthikar, J., Jiao, X., Ngambia, A., Wang, T., Khan, A., Jawad, A., Xue, Q., Liu, L., Chen, Z., 2018. Facile one-pot synthesis of sustainable Carboxymethyl chitosan – sewage sludge biochar for effective heavy metal chelation and regeneration. *Bioresour. Technol.* 262, 22–31. <https://doi.org/10.1016/j.biortech.2018.04.053>.
- Iftthikar, J., Chen, Zhuqi, Chen, Zhulei, Jawad, A., 2020a. A self-gating proton-coupled electron transfer reduction of hexavalent chromium by core-shell SBA-Dithiocarbamate chitosan composite. *J. Hazard Mater.* 384, 121257. <https://doi.org/10.1016/j.jhazmat.2019.121257>.
- Iftthikar, J., Shahib, I.I., Sellaoui, L., Jawad, A., Zhao, M., Chen, Zhuqi, Chen, Zhulei, 2020b. pH tunable anionic and cationic heavy metal reduction coupled adsorption by thiol cross-linked composite: physicochemical interpretations and fixed-bed column mathematical model study. *Chem. Eng. J.* 401, 12641. <https://doi.org/10.1016/j.cej.2020.126041>.
- Karimi-Maleh, H., Ayati, A., Davoodi, R., Tanhaei, B., Karimi, F., Malekmohammadi, S., Orooji, Y., Fu, L., Sillanpää, M., 2021. Recent advances in using of chitosan-based adsorbents for removal of pharmaceutical contaminants: a review. *J. Clean. Prod.* 291, 125880. <https://doi.org/10.1016/j.jclepro.2021.125880>.
- Kovtun, A., Campodoni, E., Favaretto, L., Zambianchi, M., Salatino, A., Amalfitano, S., Navacchia, M.L., Casentini, B., Palermo, V., Sandri, M., Melucci, M., 2020. Multifunctional graphene oxide/biopolymer composite aerogels for microcontaminants removal from drinking water. *Chemosphere* 259, 1–10. <https://doi.org/10.1016/j.chemosphere.2020.127501>.
- Lee, S.S., Bai, H., Liu, Z., Sun, D.D., 2015. Green approach for photocatalytic Cu(II)-EDTA degradation over TiO<sub>2</sub>: toward environmental sustainability. *Environ. Sci. Technol.* 49, 2541–2548. <https://doi.org/10.1021/es504711e>.
- Li, C., Yan, Y., Zhang, Q., Zhang, Z., Huang, L., Zhang, J., Xiong, Y., Tan, S., 2019. Adsorption of Cd<sup>2+</sup> and Ni<sup>2+</sup> from aqueous single-metal solutions on graphene oxide-chitosan-poly(vinyl alcohol) hydrogels. *Langmuir* 35, 4481–4490. <https://doi.org/10.1021/acs.langmuir.8b04189>.
- Li, S., Wan, Y., Guo, S., Luo, J., 2021. Ferric ions mediated defects narrowing of graphene oxide nanofiltration membrane for robust removal of organic micropollutants. *Chem. Eng. J.* 411, 128587. <https://doi.org/10.1016/j.cej.2021.128587>.
- Li, R., Kadrispahic, H., Koustrup Jørgensen, M., Brøndum Berg, S., Thornberg, D., Mielczarek, A.T., Bester, K., 2022. Removal of micropollutants in a ceramic membrane bioreactor for the post-treatment of municipal wastewater. *Chem. Eng. J.* 427, 131458. <https://doi.org/10.1016/j.cej.2021.131458>.
- Liu, X., Ma, R., Wang, Xiangxue, Ma, Y., Yang, Y., Zhuang, L., Zhang, S., Jehan, R., Chen, J., Wang, Xiangke, 2019. Graphene oxide-based materials for efficient removal of heavy metal ions from aqueous solution: a review. *Environ. Pollut.* 252, 62–73. <https://doi.org/10.1016/j.envpol.2019.05.050>.
- Lv, M., Yan, L., Liu, C., Su, C., Zhou, Q., Zhang, X., Lan, Y., Zheng, Y., Lai, L., Liu, X., Ye, Z., 2018. Non-covalent functionalized graphene oxide (GO) adsorbent with an organic gelator for co-adsorption of dye, endocrine-disruptor, pharmaceutical and metal ion. *Chem. Eng. J.* 349, 791–799. <https://doi.org/10.1016/j.cej.2018.04.153>.
- Ma, J., Zhou, G., Chu, L., Liu, Y., Liu, C., Luo, S., Wei, Y., 2017. Efficient removal of heavy metal ions with an EDTA functionalized chitosan/polyacrylamide double network hydrogel. *ACS Sustain. Chem. Eng.* 5, 843–851. <https://doi.org/10.1021/acssuschemeng.6b02181>.
- Ma, S., Si, Y., Wang, F., Su, L., Xia, C.C., Yao, J., Chen, H., Liu, X., 2017. Interaction processes of ciprofloxacin with graphene oxide and reduced graphene oxide in the presence of montmorillonite in simulated gastrointestinal fluids. *Sci. Rep.* 7, 1–11. <https://doi.org/10.1038/s41598-017-02620-4>.
- Marrakchi, F., Hameed, B.H., Hummadi, E.H., 2020. Mesoporous biohybrid epichlorohydrin crosslinked chitosan/carbon-clay adsorbent for effective cationic and anionic dyes adsorption. *Int. J. Biol. Macromol.* 163, 1079–1086. <https://doi.org/10.1016/j.ijbiomac.2020.07.032>.
- Ngambia, A., Iftthikar, J., Shahib, I.I., Jawad, A., Shahzad, A., Zhao, M., Wang, J., Chen, Zhulei, Chen, Zhuqi, 2019. Adsorptive purification of heavy metal contaminated wastewater with sewage sludge derived carbon-supported Mg(II) composite. *Sci. Total Environ.* 691, 306–321. <https://doi.org/10.1016/j.scitotenv.2019.07.003>.
- Perumal, S., Atchudan, R., Yoon, D.H., Joo, J., Cheong, I.W., 2019. Spherical chitosan/gelatin hydrogel particles for removal of multiple heavy metal ions from wastewater. *Ind. Eng. Chem. Res.* 58, 9900–9907. <https://doi.org/10.1021/acs.iecr.9b01298>.

- Qin, X., Bai, L., Tan, Y., Li, L., Song, F., Wang, Y., 2019.  $\beta$ -Cyclodextrin-crosslinked polymeric adsorbent for simultaneous removal and stepwise recovery of organic dyes and heavy metal ions: fabrication, performance and mechanisms. *Chem. Eng. J.* 372, 1007–1018. <https://doi.org/10.1016/j.cej.2019.05.006>.
- Reddy, D.H.K., Lee, S.M., 2013. Application of magnetic chitosan composites for the removal of toxic metal and dyes from aqueous solutions. *Adv. Colloid Interface Sci.* 201–202, 68–93. <https://doi.org/10.1016/j.cis.2013.10.002>.
- Repo, E., Warchol, J.K., Kurniawan, T.A., Sillanpää, M.E.T., 2010. Adsorption of Co(II) and Ni(II) by EDTA- and/or DTPA-modified chitosan: kinetic and equilibrium modeling. *Chem. Eng. J.* 161, 73–82. <https://doi.org/10.1016/j.cej.2010.04.030>.
- Repo, E., Warchol, J.K., Bhatnagar, A., 2013. Aminopolycarboxylic acid functionalized adsorbents for heavy metals removal from water. *Water Res.* 47, 4812–4832. <https://doi.org/10.1016/j.watres.2013.06.020>.
- Schwarzenbach, R.P., Escher, B.I., Fenner, K., Hofstetter, T.B., Johnson, C.A., Gunten, U., von Wehrli, B., 2006. The challenge of micropollutants in aquatic systems. *Science* (80) 313, 1072–1077.
- Shahzad, A., Miran, W., Rasool, K., Nawaz, M., Jang, J., Lim, S.R., Lee, D.S., 2017. Heavy metals removal by EDTA-functionalized chitosan graphene oxide nanocomposites. *RSC Adv.* 7, 9764–9771. <https://doi.org/10.1039/c6ra28406j>.
- Sharma, P., Singh, A.K., Shahi, V.K., 2019. Selective adsorption of Pb(II) from aqueous medium by cross-linked chitosan-functionalized graphene oxide adsorbent. *ACS Sustain. Chem. Eng.* 7, 1427–1436. <https://doi.org/10.1021/acssuschemeng.8b05138>.
- Tüüli, M., Geckeler, K.E., 1999. Synthesis and properties of hydrophilic polymers. Part 7. Preparation, characterization and metal complexation of carboxy-functional polyesters based on poly(ethylene glycol). *Polym. Int.* 48, 909–914. [https://doi.org/10.1002/\(SICI\)1097-0126\(199909\)48:9<909::AID-PI244>3.0.CO;2-E](https://doi.org/10.1002/(SICI)1097-0126(199909)48:9<909::AID-PI244>3.0.CO;2-E).
- Usman, M., Ahmed, A., Yu, B., Wang, S., Shen, Y., Cong, H., 2021. Simultaneous adsorption of heavy metals and organic dyes by  $\beta$ -Cyclodextrin-Chitosan based cross-linked adsorbent. *Carbohydr. Polym.* 255, 117486. <https://doi.org/10.1016/j.carbpol.2020.117486>.
- Vakili, M., Mojiri, A., Kindaichi, T., Cagnetta, G., Yuan, J., Wang, B., Giwa, A.S., 2019. Cross-linked chitosan/zeolite as a fixed-bed column for organic micropollutants removal from aqueous solution, optimization with RSM and artificial neural network. *J. Environ. Manag.* 250, 109434. <https://doi.org/10.1016/j.jenvman.2019.109434>.
- Verma, M., Tyagi, I., Chandra, R., Gupta, V.K., 2017. Adsorptive removal of Pb (II) ions from aqueous solution using CuO nanoparticles synthesized by sputtering method. *J. Mol. Liq.* 225, 936–944. <https://doi.org/10.1016/j.molliq.2016.04.045>.
- Verma, M., Kumar, A., Pal, K., Kumar, R., Kumar, V., Mohan, C., Rawat, V., Rao, G., Kumari, S., Sharma, P., Kim, H., 2020. One-pot hydrothermal synthesis and its use for adsorptive removal of Pb<sup>2+</sup> ions from aqueous medium. *J. Mol. Liq.* 315, 113769. <https://doi.org/10.1016/j.molliq.2020.113769>.
- Verma, M., Lee, I., Sharma, S., Kumar, R., Kumar, V., Kim, H., 2021a. Simultaneous removal of heavy metals and ciprofloxacin micropollutants from wastewater using ethylenediaminetetraacetic acid-functionalized  $\beta$ -cyclodextrin-chitosan adsorbent. *ACS Omega* 6, 34624–34634. <https://doi.org/10.1021/acsomega.1c05015>.
- Verma, M., Mitran, M., Kim, H., Vaya, D., 2021b. Efficient photocatalytic degradation of Malachite green dye using facilely synthesized cobalt oxide nanomaterials using citric acid and oleic acid. *J. Phys. Chem. Solid.* 155, 110125. <https://doi.org/10.1016/j.jpcs.2021.110125>.
- Verma, M., Tyagi, I., Kumar, V., Goel, S., Vaya, D., Kim, H., 2021c. Fabrication of GO-MnO<sub>2</sub> nanocomposite using hydrothermal process for cationic and anionic dyes adsorption: kinetics, isotherm, and reusability. *J. Environ. Chem. Eng.* 9, 106045. <https://doi.org/10.1016/j.jece.2021.106045>.
- Verma, M., Lee, I., Hong, Y., Kumar, V., Kim, H., 2022a. Multifunctional  $\beta$ -Cyclodextrin-EDTA-Chitosan polymer adsorbent synthesis for simultaneous removal of heavy metals and organic dyes from wastewater. *Environ. Pollut.* 292, 118447. <https://doi.org/10.1016/j.envpol.2021.118447>.
- Verma, M., Lee, I., Oh, J., Kumar, V., Kim, H., 2022b. Synthesis of EDTA-functionalized graphene oxide-chitosan nanocomposite for simultaneous removal of inorganic and organic pollutants from complex wastewater. *Chemosphere* 287, 132385. <https://doi.org/10.1016/j.chemosphere.2021.132385>.
- Wang, B., Zhu, Y., Bai, Z., Luque, R., Xuan, J., 2017. Functionalized chitosan biosorbents with ultra-high performance, mechanical strength and tunable selectivity for heavy metals in wastewater treatment. *Chem. Eng. J.* 325, 350–359. <https://doi.org/10.1016/j.cej.2017.05.065>.
- Wen, T., Wang, J., Yu, S., Chen, Z., Hayat, T., Wang, X., 2017. Magnetic porous carbonaceous material produced from tea waste for efficient removal of as(V), Cr (VI), humic acid, and dyes. *ACS Sustain. Chem. Eng.* 5, 4371–4380. <https://doi.org/10.1021/acssuschemeng.7b00418>.
- Yang, P., Hu, X., Tu, Y., Xu, G., Sun, L., Xie, X., 2021a. The synthesis of a DMpillar[5] arene-based porous polymer with ultrafast adsorption rate and high adsorption capacity for organic micropollutants from water. *Chem. Eng. J.* 132418. <https://doi.org/10.1016/j.cej.2021.132418>.
- Yang, Y., Zeng, L., Lin, Z., Jiang, H., Zhang, A., 2021b. Adsorption of Pb<sup>2+</sup>, Cu<sup>2+</sup> and Cd<sup>2+</sup> by sulfhydryl modified chitosan beads. *Carbohydr. Polym.* 274, 118622. <https://doi.org/10.1016/j.carbpol.2021.118622>.
- Yu, F., Sun, S., Han, S., Zheng, J., Ma, J., 2016. Adsorption removal of ciprofloxacin by multi-walled carbon nanotubes with different oxygen contents from aqueous solutions. *Chem. Eng. J.* 285, 588–595. <https://doi.org/10.1016/j.cej.2015.10.039>.
- Zhang, L., Luo, H., Liu, P., Fang, W., Geng, J., 2016. A novel modified graphene oxide/chitosan composite used as an adsorbent for Cr(VI) in aqueous solutions. *Int. J. Biol. Macromol.* 87, 586–596. <https://doi.org/10.1016/j.ijbiomac.2016.03.027>.
- Zhang, S., Li, B., Wang, Xiangxue, Zhao, G., Hu, B., Lu, Z., Wen, T., Chen, J., Wang, Xiangke, 2020. Recent developments of two-dimensional graphene-based composites in visible-light photocatalysis for eliminating persistent organic pollutants from wastewater. *Chem. Eng. J.* 390, 124642. <https://doi.org/10.1016/j.cej.2020.124642>.
- Zhao, F., Repo, E., Yin, D., Sillanpää, M.E.T., 2013. Adsorption of Cd(II) and Pb(II) by a novel EGTA-modified chitosan material: kinetics and isotherms. *J. Colloid Interface Sci.* 409, 174–182. <https://doi.org/10.1016/j.jcis.2013.07.062>.
- Zhao, F., Repo, E., Yin, D., Chen, L., Kalliola, S., Tang, J., Iakovleva, E., Tam, K.C., Sillanpää, M., 2017. One-pot synthesis of trifunctional chitosan-EDTA- $\beta$ -cyclodextrin polymer for simultaneous removal of metals and organic micropollutants. *Sci. Rep.* 7, 1–14. <https://doi.org/10.1038/s41598-017-16222-7>.